Article

Micro/nanoscaled cellulose from coffee pods do not impact HT-29 cells while improving viability and endosomal compartment after *C. jejuni* CDT intoxication

Daniele Lopez[1,2], Giovanna Panza[1], Pietro Gobbi[1], Michele Guescini[1], Laura Valentini[1], Stefano Papa[1], Vieri Fusi[2], Eleonora Macedi[2], Daniele Paderni[2], Mariele Montanari[1], Barbara Canonico[1,*]

[1] Department of Biomolecular Sciences, University of Urbino Carlo Bo, 61029 Urbino, Italy

[2] Department of Pure and Applied Sciences (DiSPeA), University of Urbino Carlo Bo, 61029 Urbino, Italy

* Corresponding author: Canonico Barbara, barbara.canonico@uniurb.it

Abstract: The food industry progressively requires innovative and environmentally safe packaging materials with increased physical, mechanical, and barrier properties. Due to its unique properties, cellulose has several potential applications in the food industry as a packaging material, stabilizing agent, and functional food ingredient. A coffee pod is a filter of cellulosic, non-rigid, ready-made material containing ground portions and pressed coffee prepared in dedicated machines. In our study, we obtained, with homogenization and sonication, cellulose micro/nanoparticles from three different coffee pods. It is known that nanoparticulate systems can enter live cells and, if ingested, could exert alterations in gastrointestinal tract cells. Our work aims to investigate the response of HT-29 cells to cellulose nanoparticles from coffee pods. In particular, the subcellular effects between coffee-embedded nanocellulose (CENC) and cellulose nanoparticles (NC) were compared. Finally, we analysed the pathologic condition (Cytolethal Distending Toxin (CDT) from *Campylobacter jejuni*) on the same cells conditioned by NC and CENC. We evidenced that, for the cellular functional features analysed, NC and CENC pre-treatments do not worsen cell response to the *C. jejuni* CDT, also pointing out an improvement of the autophagic flux, particularly for CENC preconditioning.

Keywords: coffee embedded nanocellulose; nanocellulose; *C. jejuni* CDT; HT-29 intestinal cells; vacuolar compartment; biological improving responses; mitochondrial damage

1. Introduction

Cellulose materials are "generally regarded as safe" (GRAS) as binders and thickeners in food products. However, nanocellulose materials have unique properties that can improve food quality and safety and have not received US Food and Drug Administration (FDA) approval as food ingredients. Because of their unique properties, nanoscale fibrillated cellulose and crystals have additional potential applications in the food industry as 1) packaging materials, 2) stabilizing agents, and 3) functional food ingredients [1–3]. Moreover, several studies have been published regarding the use of the material to produce edible films, act as a stabilizer, and be used as an emulsifying agent, among others [4–12].

In vitro and in vivo toxicological studies of ingested nanocellulose revealed minimal cytotoxicity and no subacute in vivo toxicity. However, ingested materials may modulate gut microbial populations or alter aspects of intestinal function not elucidated by toxicity testing, which could have significant health implications [3].

Nanocellulose may have applications in modulating digestion and the absorption of nutrients and other ingested substances. Nanocellulose materials are also potentially applicable as a non-caloric fibre source to reduce the energy density of foods like chocolate, hamburgers, and dough-based products [13,14]. In addition, some studies have suggested that using nanocellulose as a source of dietary fibres may offer a range of health benefits and assist in reducing the risk of chronic diseases [2,14].

Although cellulose, widely used as a thickener and filler in foods and drugs, has been designated as GRAS [15], as cited, nanocellulose (NC) has yet to be designated as GRAS. Several researchers found that ingested NC has slightly acute toxicity and is likely non-hazardous after small quantities of ingestion [16]. From a toxicological point of view, cellulose-based ingredients have shown excellent biocompatibility, particularly NC, which exhibits minimal cytotoxicity in a wide range of human and animal cells. Cellulose nanocrystals are employed as drug carriers in medicine [17], and their cellular uptake was demonstrated. A coffee pod is a filter of cellulosic, non-rigid, ready-made material containing portions of ground and pressed coffee prepared in dedicated machines through boiling water under pressure. Coffee is the most widely known and popular beverage globally, with more than 500 billion cups consumed annually [18]. The function of the paper filter is to store the coffee powder and allow for coffee brewing. Commercially available paper filters have characteristics corresponding to the preferences and needs of the consumer, such as size, which enables the preparation of larger or smaller volumes of coffee. The coffee pods contain a precise amount of coffee between two cellulose layers. The international coffee pod market has shown rapid growth due to consumers' inclinations towards innovation, convenience, and lifestyle changes, which have, in turn, driven the global adoption of coffee pod machines (**Figure 1A**) [19]. Even with homemade coffee pods, you can get a cup of coffee with a good yield, just like with professional espresso machines.

Recently published studies [20–23] tested how many nano plastics (NP) are released when coffee cups (or other plastic disposables) are exposed to hot water. Indeed, Hernandez and co-workers found recently that plastic teabags release billions of microparticles and nanoparticles into tea [21]. Although cellulose is a renewable, sustainable, inexpensive, eco-friendly, and safely employable polymer compared to plastics, it was recently reported that water swelling has a negative impact on cellulosic material applications in packaging [24,25] and as composite additives [26]. Indeed, this cellulose response may be temperature dependent [25] and could induce some nanoparticle release, impacting the behaviour of NC along the gastrointestinal tract and its influence on food digestion and nutrient absorption [27]. Generally, the uptake of nanoparticles by the cellular system occurs through a process known as endocytosis. It is influenced by the physicochemical characteristics of nanoparticles, such as size, shape, surface chemistry, and the employed experimental conditions [28]. Nanoparticulate systems can enter live cells, often through several endocytic pathways. Considering that passive penetration of the plasma membrane may occur as an alternative route, in that case, the internalized nanomaterials are directly transferred into the cytoplasm [28,29].
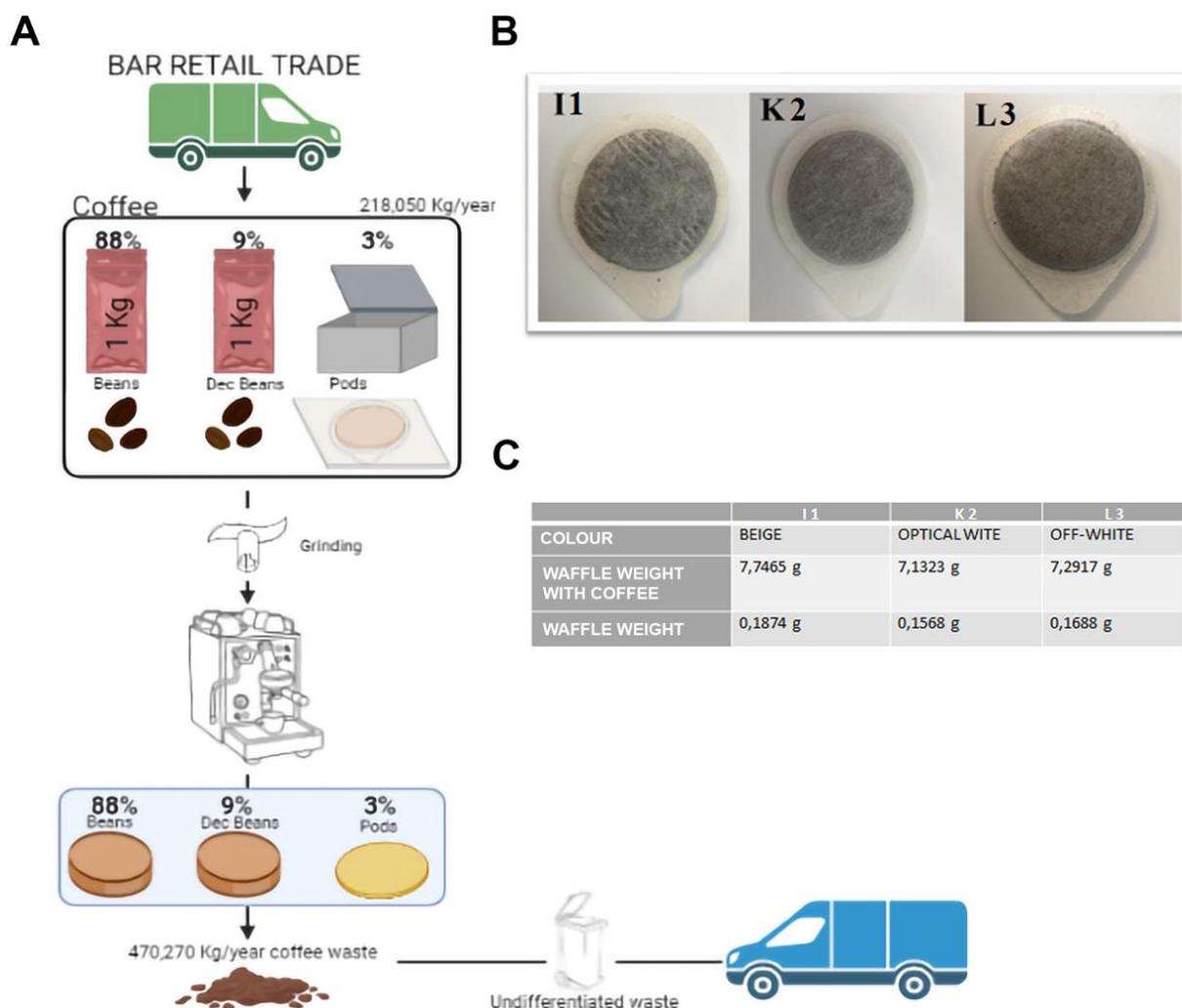
Figure 1. (A) Scheme of the path of coffee from producer to the consumer up to the disposal of the pods and highlight the relative percentages for each type (created in Biorender.com); **(B)** photos illustrating the different coffee pods we used, I1, K2, and L3; **(C)** table explaining the characteristics of paper filters, such as the color and weight of the individual waffle containing and not containing coffee.

Intestinal mucus is the first barrier for ingested nanoparticles (NPs) [30,31]. Small NPs penetrate more quickly than large ones [31]. Recently, Cao and co-workers [14] analysed the effects of cellulose nanocrystals (CNC) in different food models. They measured the volume-weighted particle size distributions in food models and oral, gastric, and small intestinal phases of digestion, exposing a tricultured small intestinal epithelium to this obtained nanoparticulate matter. They demonstrated that CNC is relatively non-cytotoxic in a triculture of human intestinal epithelium under the tested experimental conditions. Moreover, CNC in the employed food models had little impact on the triculture proteome. Therefore, several authors agree that nanocellulose's applications in the food industry need future investigations to determine its potential implications for human health.

Foodborne pathogens (bacteria, parasites, etc.) are biological agents that cause food poisoning [32], and foodborne disease is divided into two categories: infection and intoxication. Foodborne infection is associated with a prolonged incubation period; therefore, the onset of symptoms in foodborne intoxication is shorter than in

foodborne infection [33]. Gram-negative *Campylobacter jejuni* is a major cause of foodborne gastroenteritis in humans worldwide. The cytotoxic effects of *Campylobacter* have been mainly ascribed to the actions of the Cytolethal Distending Toxin (CDT) [34]. CDT is a tripartite genotoxin composed of CdtA, CdtB, and CdtC subunits [35–37]. Among them, CdtB has deoxyribonuclease activity and induces double-strand breaks (DSBs). DSB stimulates spontaneous activation of DNA damage responses, leading to cell cycle arrest. CdtB has been shown to arrest the cell cycle in the G2/M phase [37]. Indeed, we previously demonstrated [38] that CDT-treated HeLa cells increase their endolysosomal compartment because of toxin internalization, in addition to simultaneous and partial lysosomal destabilization. Indeed, in human-isolated monocytes, we found that mitochondria and lysosomes were targeted differently by CDTs from different *C. jejuni* strains [39].

We investigated the response of HT-29 cells, representing a model of goblet intestinal cells, to cellulose nanoparticles from three different typologies of coffee pods. Besides evaluating possible cytotoxic effects, we detailed the mitochondrial network and vacuolar compartment (endosome-lysosomes). Indeed, since we are investigating effects induced by cellulose from coffee pods, we treated HT-29 cells with homogenates obtained without coffee brewing (eliminating coffee powder) and homogenates of pods after coffee brewing to consider the peculiar impact of coffee embedding. The comparison of the subcellular effects between cellulose nanoparticles (NC) and coffee-embedded nanoparticles (CENC) was performed, mixing the three pod typologies, for a better interpretation of the data.

Finally, we analysed the impact (on the same endosomal-lysosomal routes) of *C. jejuni* CDT on HT-29 intestinal cells conditioned by micro/nanoscaled cellulose from coffee pods. This step enables us to verify possible differences between CENC and NC treatments in physiological conditions (w/o CDT exposure) and pathological conditions (during CDT exposure). Our work highlights that micro/nanoscaled cellulose from coffee pods does not significantly impact the viability and functions of HT-29 cells but even improves cell status/condition and endosomal compartment after *C. jejuni* CDT intoxication.

2. Materials and methods

2.1. Nanocellulose obtainment from coffee pods: I1, K2 and L3

We selected three coffee pods of the most famous brands of coffee present in Italy, to which we have assigned the acronyms I1, K2, and L3.

Coffee Embedded Nano Cellulose (CENC): coffee was prepared, taking care to recover the waffles, deprived of their coffee content prior to the homogenization of cellulose. For Nano Cellulose (NC) we used the coffee pod border (not brewing coffee). For the extraction of micro- and nanoparticles of cellulose, we used the homogenization technique through MediMachine II (CTSV, Torino) and serial filtration (**Figure S1**). For sonication, we took 7 mL of homogenate containing micro- and nanoparticles of cellulose and sonicated at 30 kHz with 100 W power for 1 h and 30 min with a UP200S Hielscher Ultrasonic Technology (Teltow, Germany) in an ice/water bath.

2.2. Growth conditions of bacterial strains and cell lysate preparation

jejuni ATCC 33291 were grown at 37 °C in a microaerobic chamber (Don Whitley Scientific, Shipley, United Kingdom) containing 85% N_2, 10% CO_2, and 5% O_2, either on blood agar (BA) plates containing Columbia agar base (Oxoid, Basingstoke, United Kingdom) supplemented with 7% (v/v) horse blood (TCS Microbiology, United Kingdom) and Campylobacter Selective Supplement (Oxoid) or in Brucella broth (Oxoid) with shaking at 75 rpm. *C. jejuni* strain was grown on BA plates for 24 h prior to use in all assays, unless otherwise stated. *C. jejuni* strain was grown in 50 mL Brucella broth (Oxoid) at 37 °C in a shaking incubator under microaerophilic conditions for 48 h. The bacterial suspensions were centrifuged at 4000 rpm for 10 min and the pellets were resuspended in 20 mL of Dulbecco's modified eagle medium (D-MEM) (Sigma-Aldrich, St Louis, MO, USA). Then, bacterial suspensions were adjusted spectrophotometrically to approximately 108 bacteria/mL and lysed by sonication (2×30 s bursts with 30 s intervals between each burst) by using a sonicator (Sonifier 450, Branson, Danbury, CT, USA). Cell debris and unlisted bacterial cells were then removed by centrifugation at 4000 rpm for 10 min. Aliquots of each lysate were sterilised by a 0.22-µm membrane filter (Millipore, Milano, Italy) and stored at −20 °C before use [40].

2.3. ESEM -EDS characterisation

Morphological characterisation of the micro- and nanoparticles was carried out using an Environmental Scanning Electron Microscope-Energy Dispersive Spectrometer (ESEM-EDS). A FEI Quanta 200 microscope (FEI, Hillsboro, OR, USA), equipped with an energy dispersive X-ray spectrometer (Edax Inc., Mahwah, NJ, USA), was used to evaluate the elemental composition of the sample. Observations were made on samples prepared in non-demineralized distilled water without any subsequent treatment after air drying at low vacuum (0.2−1.2 Torr) at a working distance of 10 mm using secondary and back-diffused electrons with a variable acceleration voltage of 12 to 25 kV. For elemental mapping, a real-time count of 100 s was used with spot mode—focused beam on discrete points of the sample, repeating the analysis 3–5 times per measurement.

2.4. NTA characterisation

For NanoSight tracking analysis (NTA), the homogenate underwent an additional 0.22 µm filtration to discriminate nanoparticles from micro particles. NTA measurements were performed with a NanoSight LM10 (NanoSight, Malvern Instruments Ltd., UK), equipped with a sampling chamber with a 640 nm laser and a Viton O-ring fluoroelastomer. The samples were injected into the sample chamber with sterile syringes until the liquid reached the tip of the nozzle. All measurements were made at room temperature (RT).

2.5. In vitro acute exposure of HT-29 cells

The HT-29 cell line is a human colorectal adenocarcinoma cell line and was cultured in RPMI 1640 Medium (Sigma-Aldrich, St Louis, MO, USA) supplemented with 10% Heat-Inactivated Foetal Bovine Serum (FBS; Gibco; Thermo Fisher

Scientific, Inc., Waltham, MA, USA), 1% L-glutamine (Sigma-Aldrich, St Louis, MO, USA), and 1% penicillin/streptomycin (Sigma-Aldrich, St Louis, MO, USA) at 37 ℃ in humidified air with 5% CO_2. Regarding experimental assays, cells were seeded in 6-well plates at a density of 1.5×10^5 cells per well. CENC and NC were added to the medium at a dilution of 1:10 for I1 and K2, and 1:9 for L3 samples, and incubated for 24 h, 48 h, 72 h and 96 h. For the negative control, the cells were incubated with medium only.

2.6. Treatment of HT-29 cells with *C. jejuni* lysates

HT-29 cells after pre-treatment with CENC and NC were incubated with 2 mL of media enriched with *C. jejuni* cell lysates (1:50 dilution) from ATCC 33291 strains previously prepared for 24 h and 72 h. Treated cells were analysed by means of flow cytometry and confocal microscopy to evaluate different cellular parameters. For the negative control, cells were incubated with media only.

2.7. Flow cytometric analyses

Cytometric experiments were performed with a FACSCanto II (BD) flow cytometer equipped with an argon laser (Blue, Ex 488 nm), a helium neon laser (Red, Ex 633 nm), and a solid-state diode laser (Violet, Ex 405 nm). The analyses were performed with the FACSDiva TM (BD) software. At least 10,000 cellular events were acquired for each sample.

Cell viability was assessed by means of Propidium Iodide (PI; Sigma-Aldrich, St Louis, MO, USA) or 7-AAD staining. The cells were incubated for 10 min in the dark with PI 1 mg/mL or with 7-AAD (Beckman Coulter, USA). We detected the percentage of PI or 7-AAD-positive events. Mitochondrial characteristics were investigated through TMRE staining. Tetra-methylrodamine ethyl ester perchlorate (TMRE) (Sigma-Aldrich, St. Louis, MO, USA) is a cationic dye that can penetrate the mitochondria, generating a red-orange fluorescence as intense as the mitochondrial membrane potential. TMRE 40 nm was added to the sample 15 min before the acquisition time. The samples were analysed by flow cytometry using the appropriate fluorescence channel [41]. LysoTracker Green or Deep Red (LTG/LTDR) dye (Thermo Fisher Scientific, USA) was used to mark and trace the lysosomes. The LysoTracker is an acidotropic and fluorescent probe that serves to monitor acidic organelles in living cells. The amount of fluorescence obtained by LysoTracker staining is directly proportional to the volume of lysosomes in the cell. LysoTracker 100 nm was used to mark the lysosomes, and after 30 min of incubation, the green or red lysosomal fluorescence was detected by flow cytometry and confocal microscopy [42]. To study the autophagic machinery, the cells were incubated with 50 μm monodansylcadaverine MDC (Sigma-Aldrich, St. Louis, MO, USA) in order to evaluate the autophagolysosomes (autophagic vacuoles). The generation of reactive oxygen species was determined by the cytometric analysis of cells labelled with CM-H2DCFDA (Thermo Fisher Scientific, USA), which can detect the generation of intracellular H_2O_2. The 5-(e-6)-chloromethyl-2,7-dichlorodihydrofluorescein diacetate acetyl ester (CM-H2DCFDA) fluorescent probe is a membrane-permeable compound that is converted into a fluorescent, impermeable compound, H2DCF, by

intracellular esterases. DCF (dichlorofluorescein) is a highly fluorescent compound produced by the oxidation of H2DCF by hydrogen peroxide. The amount of peroxide produced affects the intensity of DCF fluorescence inside the cells. CM-H2DCFDA was solubilized in dimethyl sulfoxide (DMSO) (Sigma-Aldrich, USA) and then diluted in Phosphate-buffered saline (PBS) and used at a final concentration of 5 μm for 30 min at 37 °C [43,44]. A new fluorescent probe for vesicular trafficking, the 1,7-bis-(7-nitrobenzo[1,2,5]oxadiazole-4-yl)-4,10-dimethyl-1,4,7,10-tetraazacyclododecane, called AJ2NBD [45], was used. AJ2NBD was dissolved in DMSO at the final concentration of 15 mm. Cells were incubated at 37 °C with 500 nm (f.c.) of AJ2NBD for 20 min [46]. In order to quantify the vesicular trafficking in treated cells, HT-29 cells were incubated in complete culture medium and stained at different time points from 0 to 1 day with the specific probe AJ2NBD (500 nm for 20 min).

2.8. Confocal microscopy

To evaluate the behaviour of different probes, the cells were grown on MatTek glass bottom chambers (MatTek Corporation) and then stained with fluorescent probes. To evaluate the vesicular trafficking in treated cells, HT-29 cells were incubated in complete culture medium with the specific probe AJ2NBD (500 nm for 20 min), and the vesicular compartment was studied by confocal microscopy at different time points from t0 (after incubation of AJ2NBD) up to 1 day. To evaluate the lysosomal formation, the cells were stained with LysoTracker Deep Red (LTDR) at 100 nm. The images were acquired by a Leica TCS SP5 II confocal microscope (Leica Microsystem, Germany) with 488, 543, and 633 nm illumination and oil-immersed objectives and averaged in real time using a line average to reduce random noise. The images were further processed and analysed in ImageJ software (National Institutes of Health, Bethesda, MD, USA).

2.9. Statistical analyses

Data are shown as the mean (or percentage, as indicated) ± standard deviation (SD) of at least three independent experiments. The means of two groups were compared using a *t* test. The *p* values less than 0.05 were considered statistically significant. Analysis of variance (ANOVA) approaches were used to compare values among more than two different experimental groups for data that met the normality assumption. One-way ANOVA or two-way ANOVA were followed by a Bonferroni post-hoc test. The *p* values less than 0.05 were considered statistically significant. Bonferroni's multiple comparison test revealed statistical significance: * = $p < 0.05$, ** = $p < 0.01$, *** = $p < 0.001$, **** = $p < 0.0001$. All statistical analyses were performed using GraphPad Prism 9.0.0 (GraphPad software, San Diego, CA, USA).

3. Results

3.1. Nanocellulose evaluation by ESEM and NanoSight characterisation

We selected three types of coffee pods (I1, K2, L3). A first evaluation of the pods was made macroscopically based on the physical and morphological characteristics of

the coffee waffle, in particular the size (weight) and the colour (**Figure 1C**). As reported in the materials and methods section, we obtained two types of nanocellulose: Coffee Embedded Nano Cellulose (CENC) and Nano Cellulose (NC). We characterized 1) the presence of micro- and cellulose nanoparticles, and then 2) we evaluated whether the use of sonication improved the yield of nanoparticles. ESEM data show the best morphological uniformity in the homogenate samples than in the homogenization + sonication procedure (**Figure 2A**). Consequently, we continue the analyses on the nanoparticles obtained by the unique homogenization step. We evaluated the size and morphology of cellulose nanoparticles by NTA (**Figure 2B**). From NTA and ESEM, the average size of the nanoparticles obtained by the homogenization technique is 80 nm (**Figures 2A** and **2B**). The ESEM-EDS elemental analysis peaks showed the presence of sulfur (S) (**Figure 2C**). Hydrochloric and sulfuric acids have been extensively used to obtain cellulose from wood [47]. Sulfuric acid hydrolysis of native cellulose fibres causes the breakdown of the fibres into rod-like fragments [48]. During the hydrolysis by sulfuric acid, negatively charged sulfate groups will be introduced on the cellulose chain through the esterification of hydroxyls [47]. For this reason, the presence of sulphur must be considered normal based on wood treatment to obtain cellulose. We evaluated each homogenate's dry weight (**Figure 2D**) to gain further knowledge of the concentration of our homogenates. The results obtained (**Figure 2E**) were assessed as a value of μg/mL. However, besides such quantitative assessment, we performed the nanoparticle counts employing NTA (**Figure 2F**), obtaining the particle concentration/mL that we equally administered to HT-29 cells.
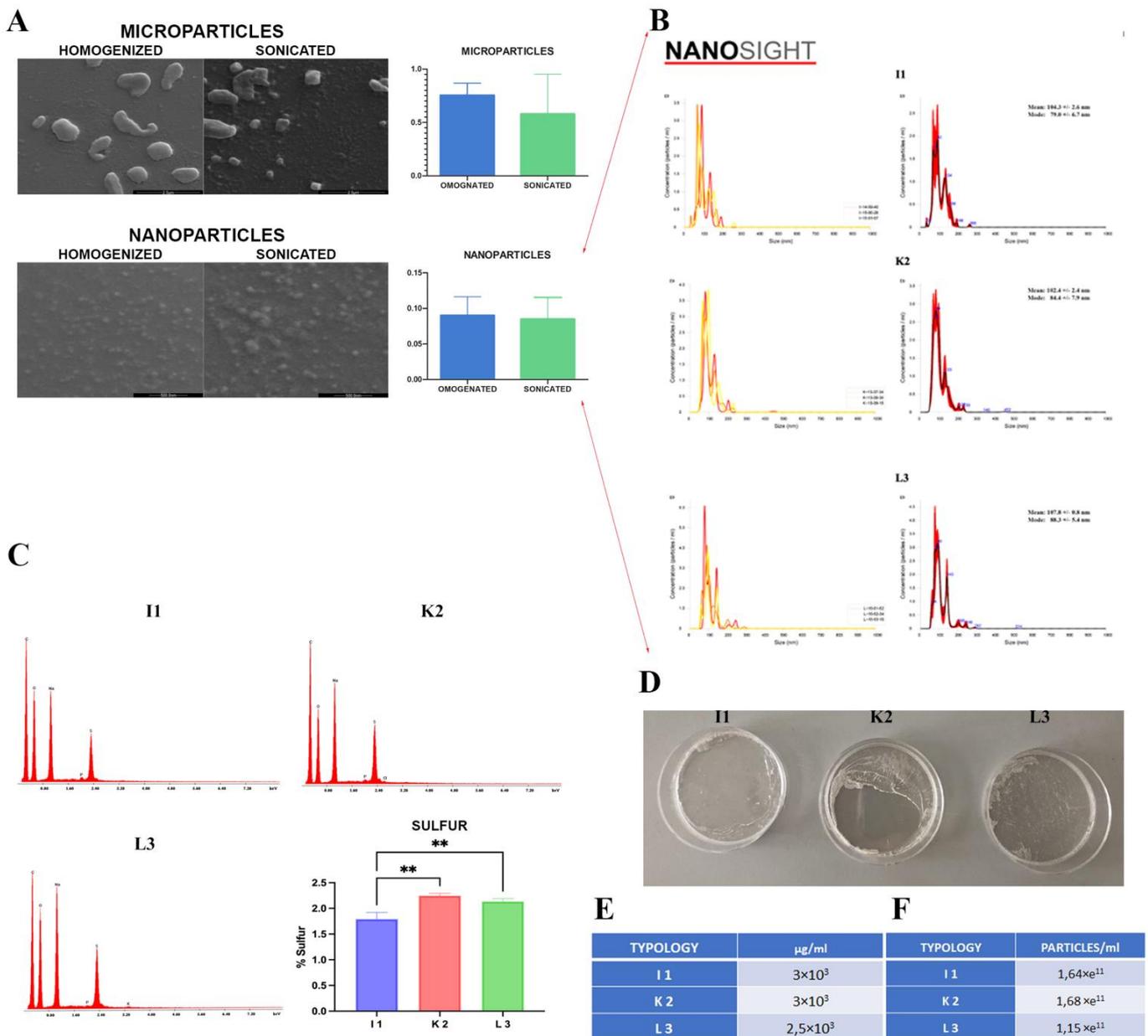
Figure 2. (A) ESEM analysis of microparticles and nanoparticles obtained by homogenization and by homogenization and sonication. Histograms reveal the size of microparticles and nanoparticles with the *T*-test assessments (*P* value to two tails); **(B)** NTA of the size distribution of the different types of pods (I1, K2, L3); **(C)** EDS spectra for homogenates I1, K2, L3 and histogram evaluating the percentage of Sulphur present in homogenates. One-way ANOVA with Bonferroni's multiple comparison tests revealed a significant difference: ** = $p < 0.01$; **(D)** photos of the homogenates of micro- and nanoparticles/fibrils in Petri dishes following complete evaporation of the liquid medium (fore dry weight of micro- and nanoparticles/fibrils); **(E)** table reporting the concentration in μg/mL for each type of micro and nanoparticles/fibrils analyzed by the dry weight; **(F)** table reporting the number of particles per mL by NanoSight.

3.2. Intestinal cell response to nanosized cellulose (NC) and to coffee embedded nanosized cellulose (CENC)

The most important factors influencing recognition, uptake, and cellular response include nanocellulose size, length of fibres, shape, surface area and charge, degree of

agglomeration in biological media, source, and type of nanocellulose [49]. In our model, all these features are identical for CENC and NC samples, varying only for the presence of the imbibition of the cellulose by coffee brewing.

Cell viability

Although nanocellulose is largely considered non-toxic in its bulk form, different authors reported that chronic cell exposure to high concentrations of nanocellulose may result in an apoptotic cellular response [50]; moreover, coffee has the ability to trigger apoptosis by modulating multiple components of the apoptotic response [51,52]. Cell death was assessed using supravital propidium iodide (supravital PI). We did not detect any relevant cell death induction or significant differences in CENC and NC-treated cells with respect to control (**Figure 3A**,**C**), (**Figure 3B**,**D**) for the investigated time points. In detail, after 24 h of exposure, CENC-treated cells (I1, K2, L3) appear to maintain viable conditions as in the control. The analyses showed that, compared with control cells, the treatment with CENC and NC did not cause any significant increase in the percentage of PI-positive cells. Indeed, CENC-treated HT-29 cells revealed, after 24 h and 72 h, lower PI positivity than control samples (**Figure 3B**).
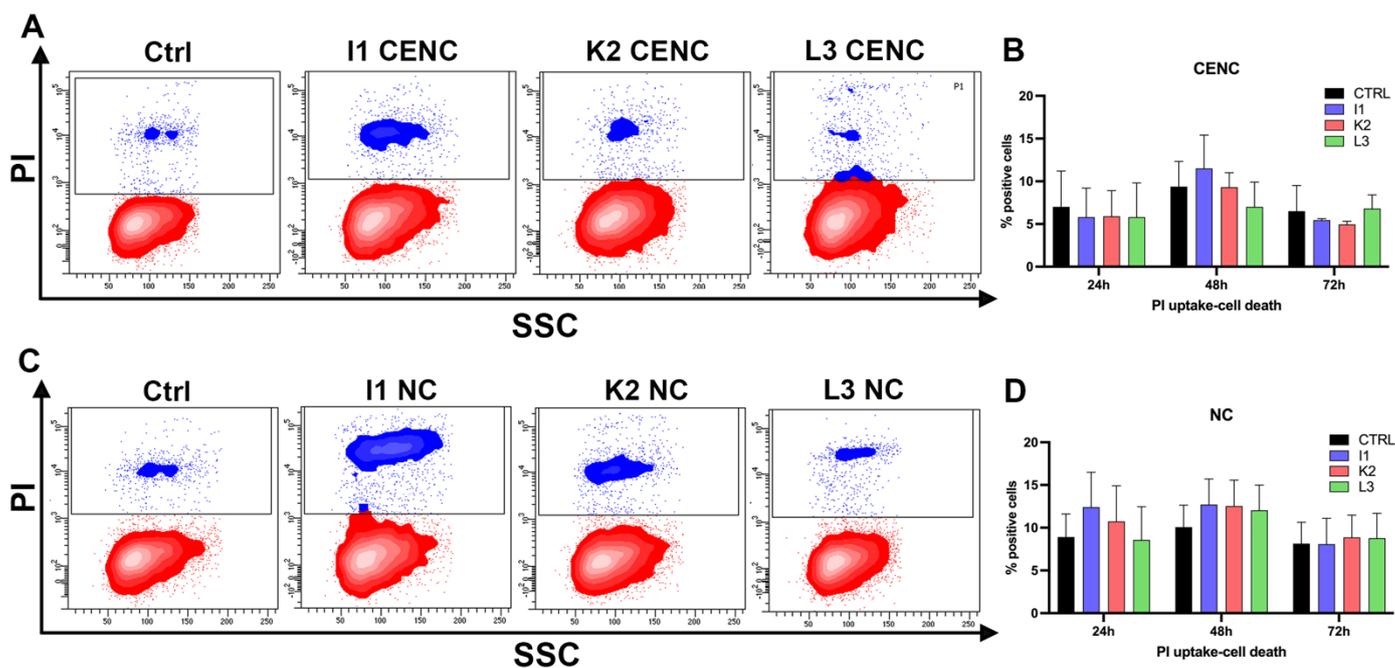
Figure 3. (A) Contour plot SSC vs PI from HT-29 control cells, I1 CENC HT-29 treated cells, K2 CENC HT-29 treated cells, L3 CENC HT-29 treated cells at 48 h. The rectangular region identifies events with high PI uptake (cell death); **(B)** percentages of PI-positive HT-29 cells for each CENC experimental condition from 24 h to 72 h; **(C)** contour plot SSC vs. PI from HT-29 control cells, I1 NC HT-29 treated cells, K2 NC HT-29 treated cells, and L3 NC HT-29 treated cells at 48 h. High PI uptake reveals cell death; **(D)** percentages of PI-positive HT-29 cells for each NC experimental condition from 24 h to 72 h.

3.3. Mitochondrial oxidative stress and autophagolysosome modulation in cells treated by the tree different CENC and NC types of pods

Mitochondrial membrane potential was investigated through TMRE staining, a cationic dye able to penetrate the mitochondria and generate a red-orange fluorescence

as intense as the mitochondrial membrane potential (MMP). **Figure 4** highlights a comparison between HT-29 cell MMP after administration of the three typologies of nanosized cellulose (NC) and coffee embedded nanosized cellulose (CENC). We did not observe relevant and significant differences between exposure to NC and CENC, except for L3 at the longest times (72 h and 96 h, **Figure 4A**,**D**, respectively), revealing a significant increase in mitochondria hyperpolarization in NC samples.
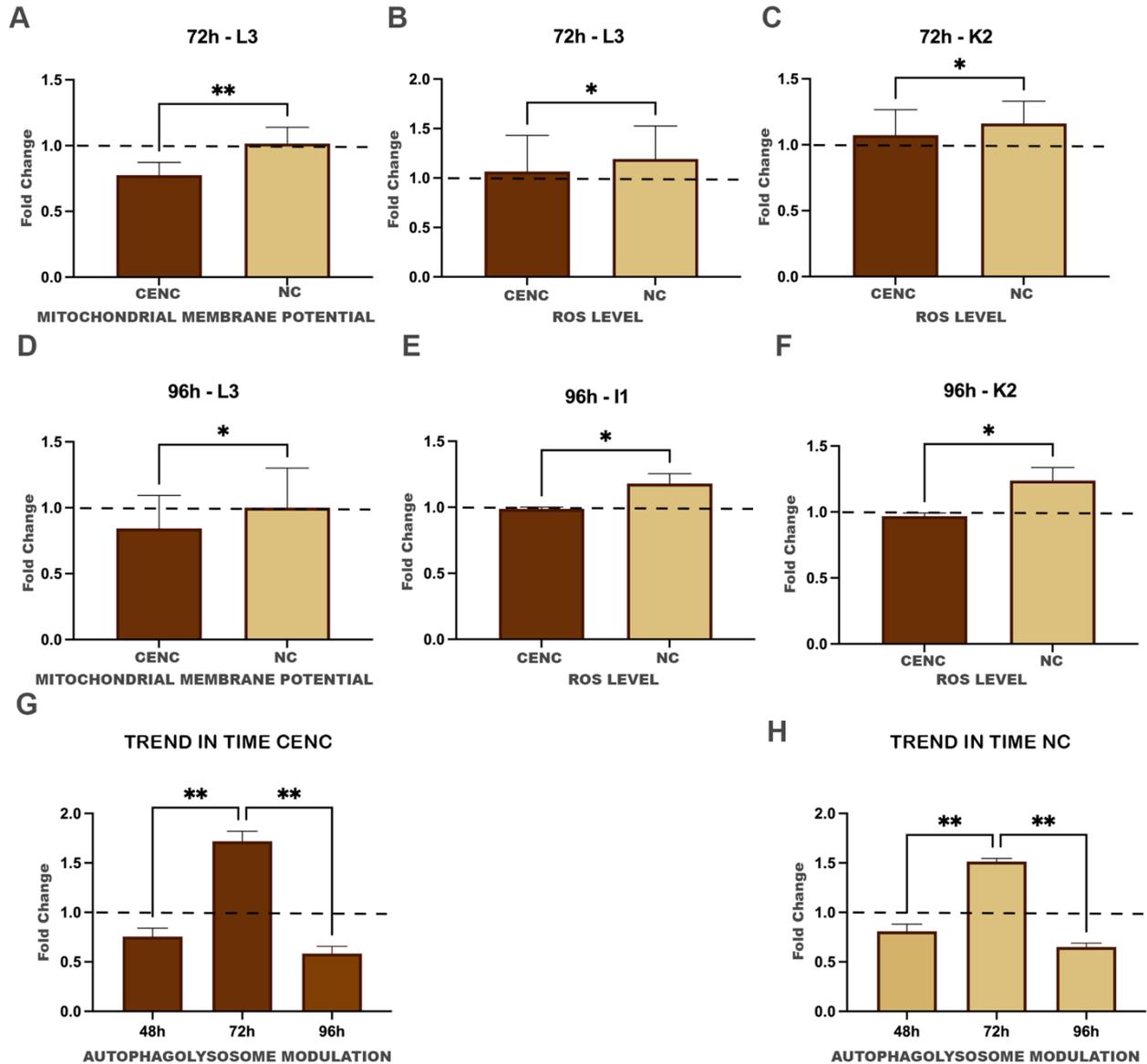
Figure 4. Fold change of: **(A)** TMRE intensity relative to untreated HT-29 cells (ctrl) for L3 CENC-treated HT-29 cells and L3 NC-treated HT-29 cells at 72 h; **(B)** DCF intensity relative to untreated HT-29 cells for L3 CENC-treated HT-29 cells and L3 NC-treated HT-29 cells at 72 h; **(C)** DCF intensity relative to untreated HT-29 cells for K2 CENC-treated HT-29 cells and K2 NC-treated HT-29 cells at 72 h; **(D)** TMRE intensity relative to untreated HT-29 cells for L3 CENC-treated HT-29 cells and L3 NC-treated HT-29 cells at 96 h; **(E)** DCF intensity relative to untreated HT-29 cells for I1 CENC-treated HT-29 cells and I1 NC-treated HT-29 cells at 96 h; **(F)** DCF intensity relative to untreated HT-29 cells for K2 CENC-treated HT-29 cells and K2 NC-treated HT-29 cells at 96 h. Fold change of autophagic-like vacuoles (MDC) intensity relative to untreated HT-29 cells (ctrl) for CENC-treated HT-29 cells; **(G)** NC-treated HT-29 cells **(H)** 48 h to 96 h. T-test and One-way ANOVA with Bonferroni's multiple comparison tests revealed significant differences $*$ = $p < 0.05$, $**$ = $p < 0.01$.

To evaluate changes in the amount of intracellular reactive oxygen species (ROS), H_2O_2 was targeted by means of CM-H2DCFDA (DCF). These evaluations are further coupled with data on MMP, in agreement with the findings of several researchers [53–56].

Histograms B and C in **Figure 4** show higher hydrogen peroxide concentrations in specific NC samples, lacking in CENC samples, in agreement with the antioxidant activity of coffee. Higher ROS amounts were registered for L3 and K2 NC-treated cells after 72 h (**Figure 4B**,**C**), whereas after 96 h, H_2O_2 increased significantly in I1 NC-treated cells.

The two major cellular sites of ROS production are the electron transport chain in mitochondria and endosomes via the NOX2-oxidase enzyme [57]. Therefore, to verify possible modulations of autophagic-like vacuoles, we investigated the intracellular presence of autophagosomes with Monodansylcadaverine (MDC). Our data show that CENC and NC-treated cells show a progressive increase of autophagic-like vacuoles at 72 h (**Figure 4G**,**H**). Of note, at 96 h, both CENC and NC-treated cells show a decrease in MDC fluorescence, suggesting that cells were able to clear the excess of autophagosomes. We did not detect any significant differences in time trends of CENC and NC samples, revealing that autophagic vacuole increase is mainly primed by nanocellulose internalisation and the modulation is essentially dependent on time and not coffee.

Autophagy is a lysosome-mediated intracellular biological degradation process [58]. For this reason, we also investigated lysosome networks. Indeed, the cellular uptake of CENC and NC particles in HT-29 cells may lead to direct lysosome damage. To assess lysosome integrity, we used a lysosomotropic dye (Lysotracker Deep Red, LTDR), analysed by flow cytometry and confocal microscopy (**Figure 5**). Moreover, we coupled these analyses to AJ2NBD (**Figure 5C**), useful in intracellular vesicular organelle detection [46]. AJ2NBD is a new dye containing the 7-nitrobenzo[1,2,5]oxadiazole-4-yl (NBD) fluorophore [59] synthesised (and patented) by Fusi and co-workers [45].

Flow cytometry highlights a not-significantly lower MFI (Mean Fluorescence Intensity) registered for K2 and L3-treated samples in respect to controls, whereas confocal images illustrate in detail AJ2NBD and LTDR co-staining.
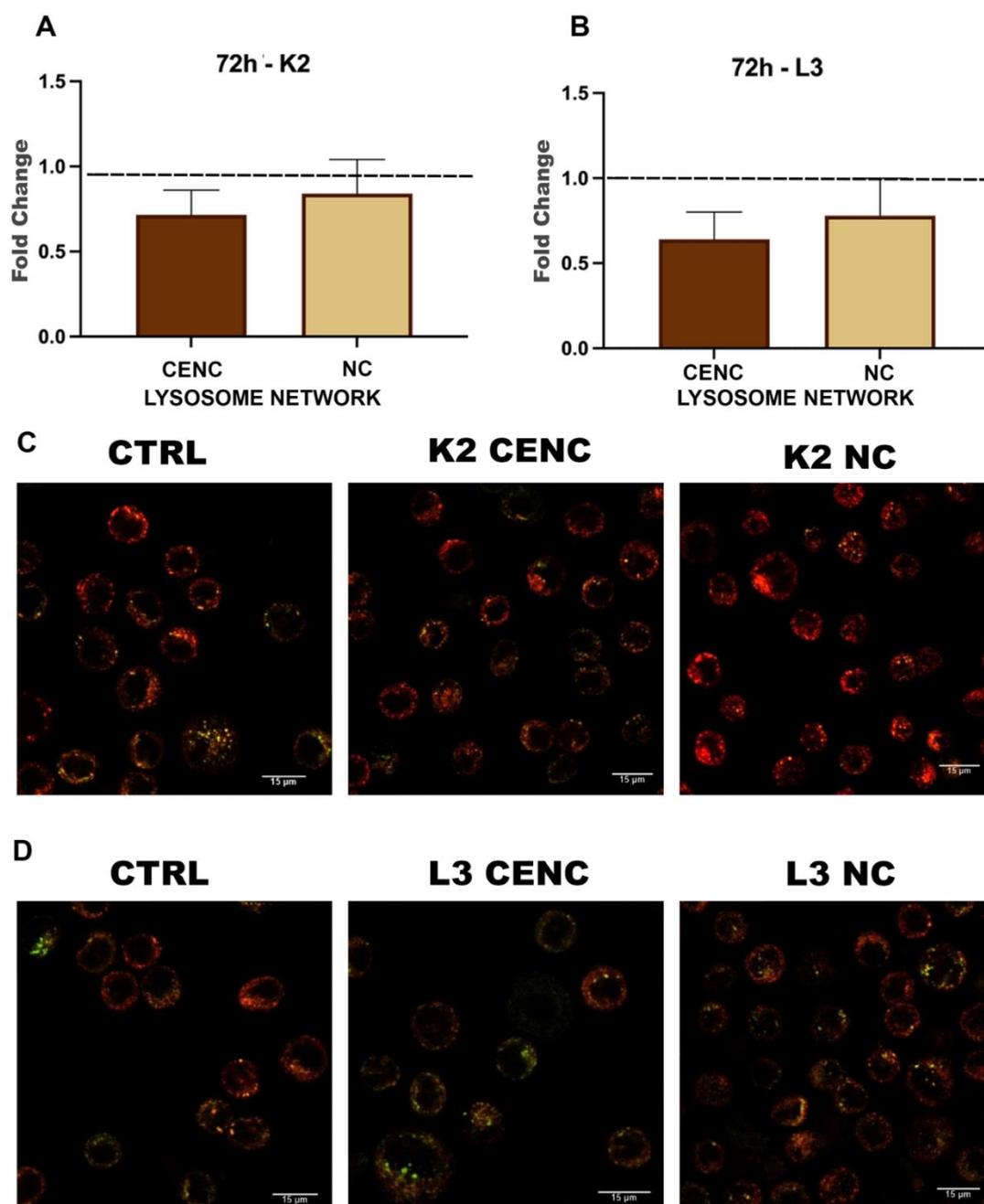
Figure 5. (A) Fold change of: LTDR intensity relative to untreated HT-29 cells (ctrl) for K2 CENC-treated HT-29 cells and K2 NC-treated HT-29 cells at 72 h; **(B)** LTDR intensity relative to untreated HT-29 cells (ctrl) for L3 CENC-treated HT-29 cells and L3 NC-treated HT-29 cells at 72 h; **(C)** Confocal images of AJ2NBD (green) and Lysotracker Deep Red (LTDR, red) fluorescence from HT-29 control cells (CTRL), K2 CENC-treated HT-29 cells and K2 NC-treated HT-29 cells, after 72 h of treatments. Scale bar: 15 µm; **(D)** Confocal images of AJ2NBD (green) and Lysotracker Deep Red (LTDR, red) fluorescence from HT-29 control cells (CTRL), L3 CENC-treated HT-29 cells and L3 NC-treated HT-29 cells, after 72 h of treatments. Scale bar: 15 µm.

3.4. Evaluation of DNA content and cell cycle profiles in cells treated by CENC and NC preparations

Finally, we evaluated the DNA content of samples treated with the three different coffee pod types (**Figure 6**). The statistical evaluation of S and G2/M phases at 72 h for both CENC and NC treatments did not highlight significant differences, except for

K2 treatments. In detail, after K2-CENC treatment, HT-29 cells revealed a mild but significant increase in S phase events, whereas after K2-NC treatment, G2/M phase events appeared to have mildly increased. This finding could arise from the highest sulphur content detected in these specific coffee pods, as shown in **Figure 2C**. In fact, different authors [60] published on the biologic effects of sulphur compounds that can inhibit or delay the cell cycle progression [61]. The overall data suggest that ingested NC has negligible toxicity, even at the massive concentrations used in our study. Moreover, coffee embedding demonstrates that it can further modulate the NC effects, even improving the baseline condition of the control, as demonstrated by the PI data as well as by other studies on coffee biologic effects [62]. Coffee includes a wide array of components that can have potential implications for health. In particular, the vast array of components included in the brewed product and the varied effects of each compound drastically limit the understanding of its physiological effects. A scheme of the most represented compounds is shown in **Figure S2**. Nevertheless, we want to underline that in our model, coffee is present in scarce amounts, derived from cellulose embedding.
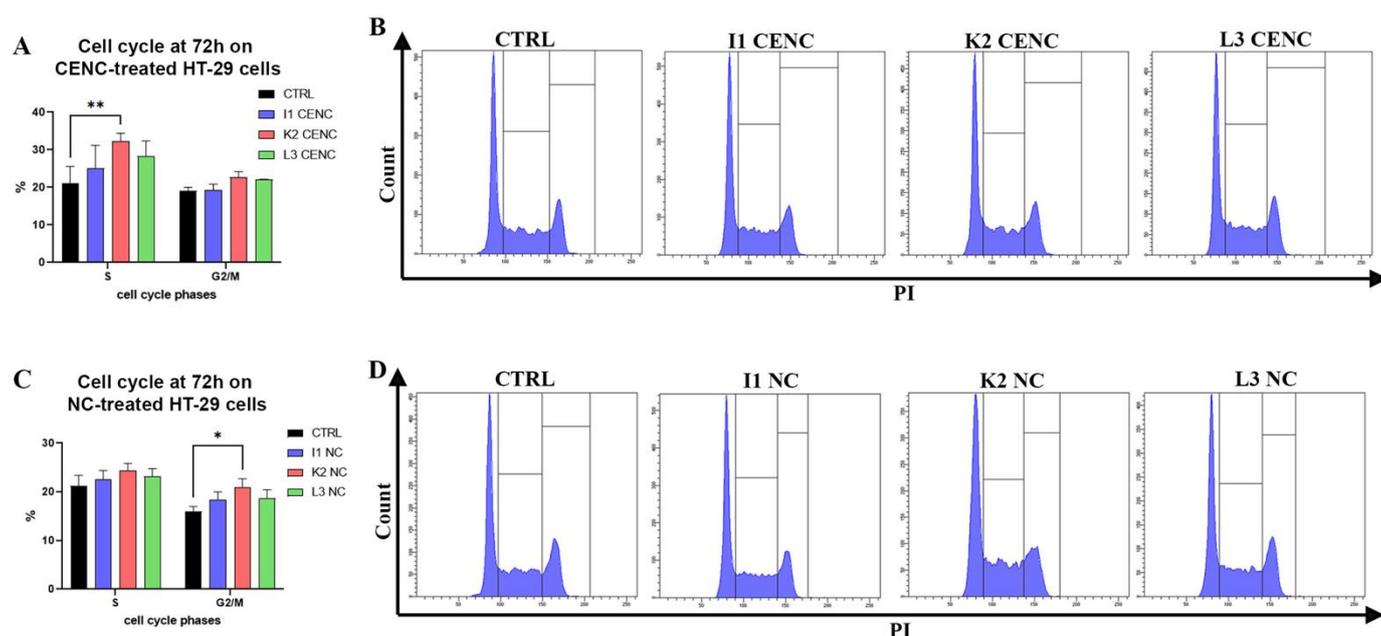
Figure 6. (A) Statistical histogram of the cell cycle phases was calculated by FC via PI staining at 72 h for HT-29 control cells and I1, K2, and L3 CENC HT-29 treated cells; **(B)** FC histograms representing the HT-29 cell population in the S and G2/M phases of the cell cycle after 72 h of I1, K2, L3 CENC administration; Two-way ANOVA with a Bonferroni's multiple comparison test revealed a significant difference (**$p < 0.01$); **(C)** Statistical histogram of the cell cycle phases at 72 h for HT-29 control cells, I1/K2/L3 NC HT-29 treated cells; Two-way ANOVA with a Bonferroni's multiple comparison test revealed a significant difference (*$p < 0.05$); **(D)** FC markers represent the HT-29 cell population in the S and G2/M cell cycle phases after 72 h of I1, K2, and L3 NC administration.

3.5. Cell response to CDT in mixed NC- and CENC-treated intestinal cells

3.5.1. Evaluation of cell viability during the time course

In this step of the study, we considered the exposure of intestinal cells to *C. jejuni* CDT-containing lysate. We mixed the homogenates from the three different coffee

pods in a unique formulation to correlate only two main groups (NC and CENC). This mixing is also justified by the lack of striking differences between the three different coffee pods (I1, K2, L3). Our data did not reveal any significant cytotoxic effects of the NC and CENC treatments; indeed, positive PI events after 24 h of NC administration were even lower than in control cells (**Figure 7A**). At 72 h the cells treated with CENC and NC show a slight increase in dead cells but are still not significant (**Figure 7B**). As observed in other cell lines [34,38,39,63], the ATCC lysate did not induce in HT-29 cells an important necrotic/apoptotic effect after 24 h (**Figure 7**); however, previous conditioning with CENC treatment showed a reduction in cell death percentages (**Figure 7C**).

After 72 h, we found a mild, although significant, increase in cell death after ATCC CDT lysate administration (**Figure 7D**), observing a decrease in dead cells in NC and CENC pretreated samples. In agreement with our previous research [34,38,39,63] and literature [64–67], the type and timing of CDT-induced cell death depend on the cell type, requiring at least 24 h to be observed.
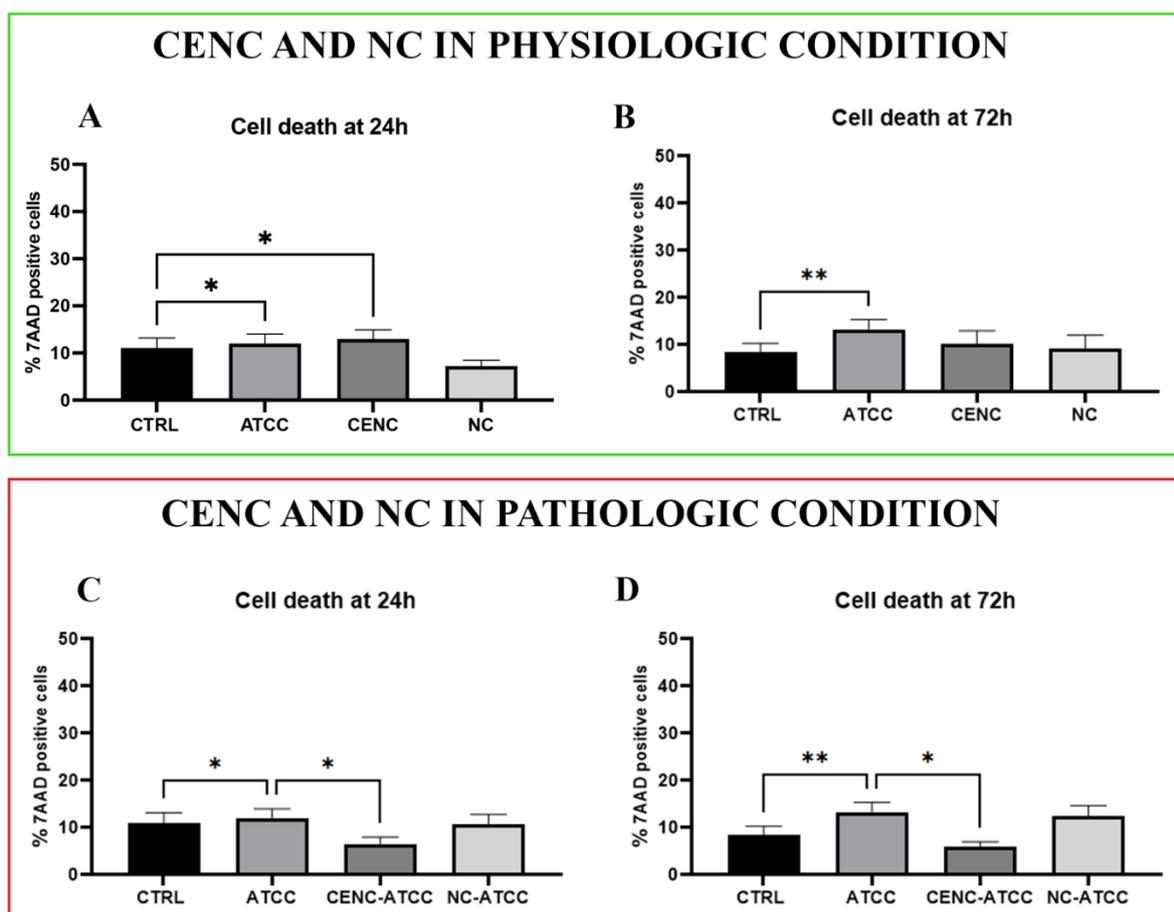
Figure 7. In the green square, % dead cells in physiological condition: **(A)** statistical histogram at 24 h on HT-29 untreated cells (CTRL), ATCC treated cells, CENC, NC; **(B)** statistical histogram at 72 h on HT-29 untreated cells (CTRL), ATCC treated cells, CENC, NC. In the red square, % dead cells in pathological condition: **(C)** statistical histogram at 24 h on HT-29 untreated cells (CTRL), ATCC treated cells, ATCC + CENC, and ATCC + NC; **(D)** statistical histogram at 72 h on HT-29 untreated cells (CTRL), ATCC treated cells, ATCC + CENC, and ATCC + NC; One-way ANOVA with Bonferroni's multiple comparison test revealed significant differences (*$p < 0.05$, **$p < 0.01$, ***$p < 0.001$).

3.5.2. Short term analyses of subcellular effects: 24 h

We evaluated intracellular ROS levels, mainly hydrogen peroxide, as shown in **Figure 8A**,**C**. Since mitochondria are one of the main producers of ROS, we contemporary assessed the MMP (**Figure 8B**). HT-29 intestinal cells slightly decrease MMP to a similar extent after NC and CENC treatment, in both groups, i.e., with and without CDT-containing lysate exposure (**Figure 8,D**).

Cellulose conditioning slightly decreases MMP, to a similar extent for control and CDT-poisoned cells **(Figure 8B,D)** [68]. Indeed, the possible impact of nanocellulose on MMP has been reported by Ventura et al. [69], describing the entry of nanoparticles and nanofibers into the mitochondrial outer membrane, causing an initial disturbance in mitochondrial activity [70].
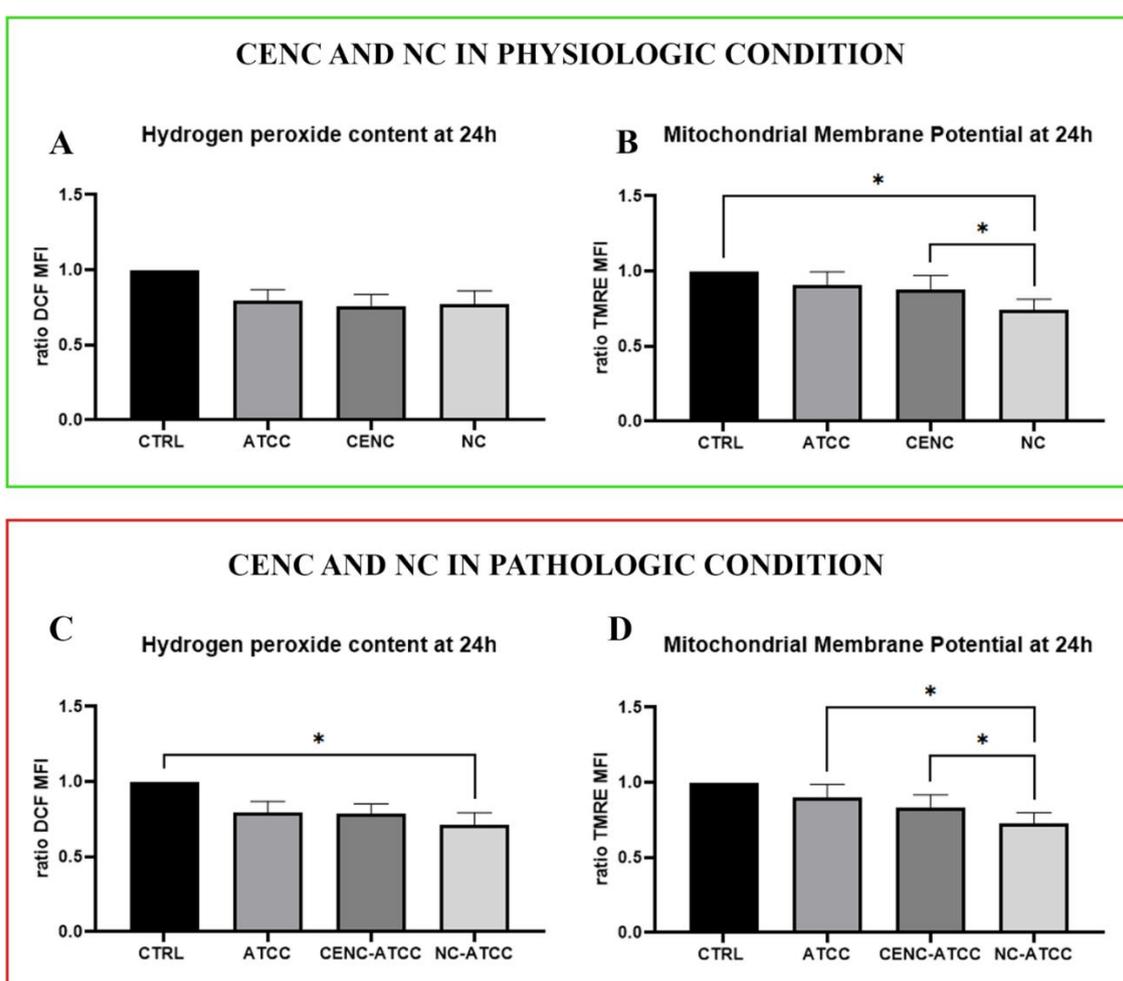
Figure 8. In the green square, the status of MMP and ROS levels in physiological conditions: (**A**) statistical histogram of ROS levels at 24 h on HT-29 untreated cells (CTRL), ATCC treated cells, CENC, and NC; expressed as fold of change of treated cells/CTRL cells of DCF MFI; (**B**) statistical histogram of MMP levels at 24 h on HT-29 untreated cells (CTRL), ATCC treated cells, CENC, and NC.; expressed as fold of change of treated cells/CTRL cells of TMRE MFI In the red square, the status of MMP and ROS levels in pathological conditions; in the red square, the status of MMP and ROS levels in pathological condition: (**C**) statistical histogram of ROS levels at 24 h on HT-29 untreated cells (CTRL), ATCC treated cells, ATCC+CENC, and ATCC+NC; (**D**) statistical histogram of MMP levels at 24 h on HT-29 untreated cells (CTRL), ATCC treated cells, ATCC+CENC, and ATCC+NC. One-way ANOVA with Bonferroni's multiple comparison tests revealed significant differences (*$p < 0.05$, **$p < 0.01$, ***$p < 0.001$).

Finally, autophagic-like vesicles, labelled by means of an MDC probe, did not show any relevant modifications among CENC, NC, and the untreated cells during short-term analyses (**Figure 9A**). To evaluate the autophagic features, we coupled lysosomal network detection to intracellular vesicle determination by means of LTDR and AJ2NBD (a new patented dye), respectively, in both NC and CENC-treated cells, with and without CDT infection (**Figure 9**).

Cytometric data report conditions similar to control cells in NC and CENC-treated cells, both for autophagosomes (**Figure 9A**) and lysosomes (**Figure 9B**). In **Figure 9C,** the AJ2NBD labelling highlights only a slight but significant decrease in ATCC-treated HT-29 cells. Contemporary findings showed that the ATCC CDT lysate induced an accumulation of autophagic-like vacuoles (**Figure 9A,D).** In pathological conditions, treatment with NC appears to weakly and significantly counteract the effects of CDT. Statistical histograms revealed that the lysosomal compartment decreased after ATCC CDT administration; on the contrary, NC conditioning limited this phenomenon (**Figure 9E**). Vesicular trafficking does not appear altered in NC and CENC samples (**Figure 9F**). Confocal images of AJ2NBD and LTDR co-labelling show a similar distribution of green vesicles in untreated cells and cells treated by CENC and NC (**Figure 9G**, upper). After ATCC conditioning, clustered and perinuclear green vesicles are visible, and LTDR RED fluorescence almost disappears; indeed, no colocalization is appreciable (**Figure 9G**). Of note, as quantified by flow cytometry, CENC and NC pretreatment rescue cells from lysosome acidity loss, and yellow fluorescence (merging green and red organelles) suggests a priming of the AJNBD+ vesicles towards lysosomal features.
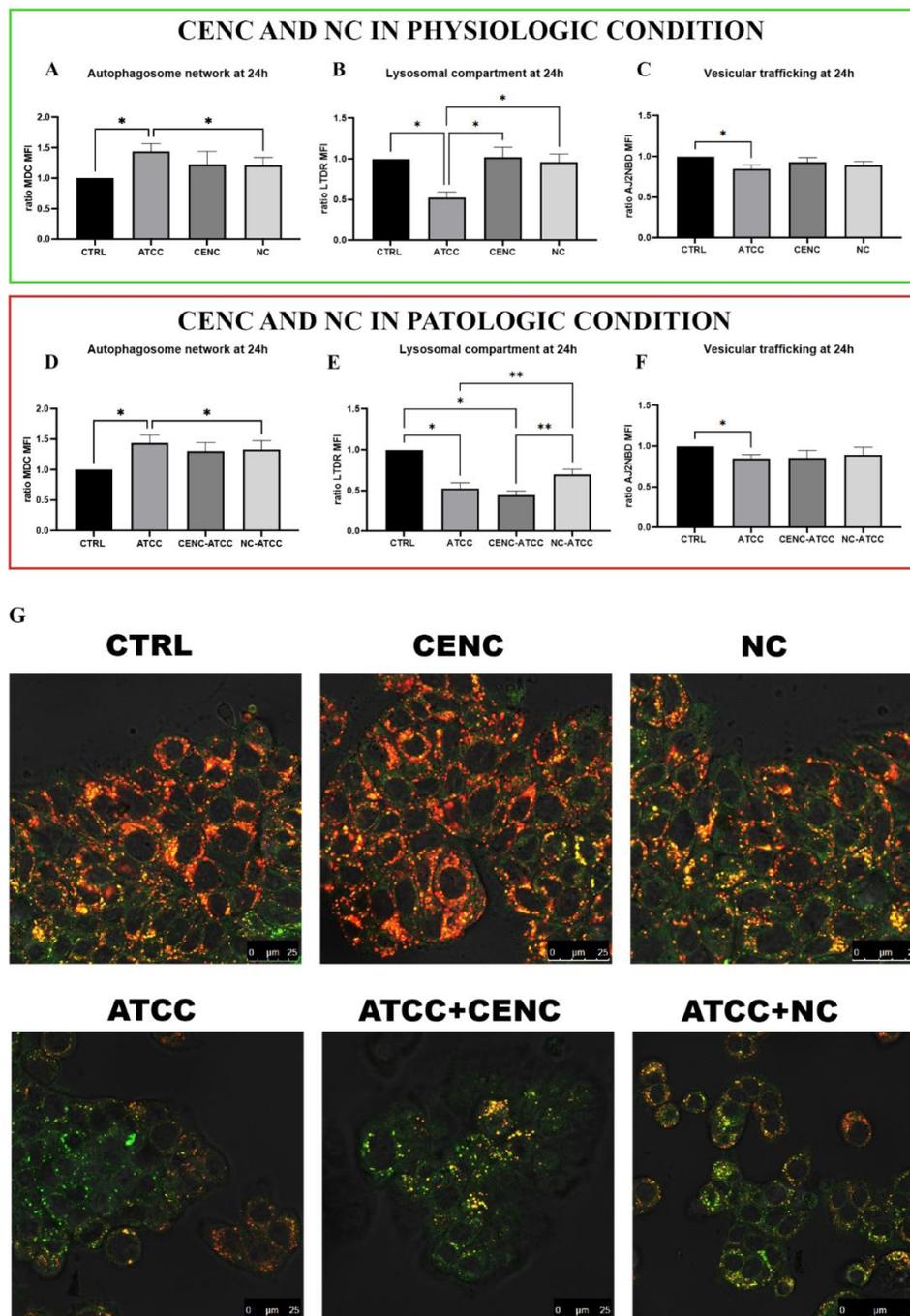
Figure 9. In the green square, the status of lysosomal and vesicular compartment in physiological conditions: (**A**) statistical histogram of autophagic-like vacuole at 24 h on HT-29 untreated cells (CTRL), ATCC treated cells, CENC, and NC; expressed as fold of change of treated cells/CTRL cells of MDC MFI; (**B**) statistical histogram of the lysosomal compartment at 24 h on HT-29 untreated cells (CTRL), ATCC treated cells, CENC, and NC; expressed as fold of change of treated cells/CTRL cells of LTDR MFI; (**C**) statistical histogram of vesicular compartments at 24 h on HT-29 untreated cells (CTRL), ATCC treated cells, CENC, and NC.; expressed as fold of change of treated cells/CTRL cells of AJ2NBD MFI; In the red square, the status of lysosomal and vesicular compartment in pathological conditions: (**D**) statistical histogram of autophagic-like vacuole at 24 h on HT-29 untreated cells (CTRL), ATCC treated cells, CENC, and NC; (**E**) statistical histogram of the lysosomal compartment at 24 h on HT-29 untreated cells (CTRL), ATCC treated cells, CENC, and NC; (**F**) statistical histogram of vesicular compartments at 24 h on HT-29 untreated cells (CTRL), ATCC treated cells, ATCC + CENC, and ATCC + NC. One-way ANOVA with Bonferroni's multiple comparison tests revealed significant differences (*$p < 0.05$, **$p < 0.01$, ***$p < 0.001$); (**G**) confocal images of AJ2NBD (green) and Lysotracker Deep Red (LTDR, red) fluorescence on HT-29 untreated cells (ctrl), cells in physiological condition treated with CENC, NC, ATCC, and cells in pathological condition ATCC + CENC and ATCC + NC after 24 h of treatments.

3.5.3. Long term analyses of subcellular effects: 72 h

After 72 h, ROS levels demonstrated a significant reduction between untreated, control, and ATCC-CDT-infected cells. Unexpectedly, CENC-ATCC samples (**Figure 10**) revealed ROS rising at 72 h, whereas no increase in ROS was detected in NC-ATCC-infected HT-29 cells. This finding propelled us to consider the properties of coffee [71,72]. It is known that coffee exhibits antioxidant and pro-oxidant properties [73]. Coffee varieties also influence the antioxidant/pro-oxidant capacities. Several bioactive molecules are present in coffee; among these, caffeine displays significant antioxidant activity, protecting membranes from oxidative damage [74] at millimolar concentrations, whereas there is no antioxidant activity present in caffeine at micromolar concentrations [75]. Furthermore, it is important to consider that the coffee traces act directly on intestinal cells without the insertion of an oral phase (as normally happens in the case of regular coffee consumption). Our data appear in agreement with [76], describing the prooxidative action of regular coffee samples during the intestinal phase.
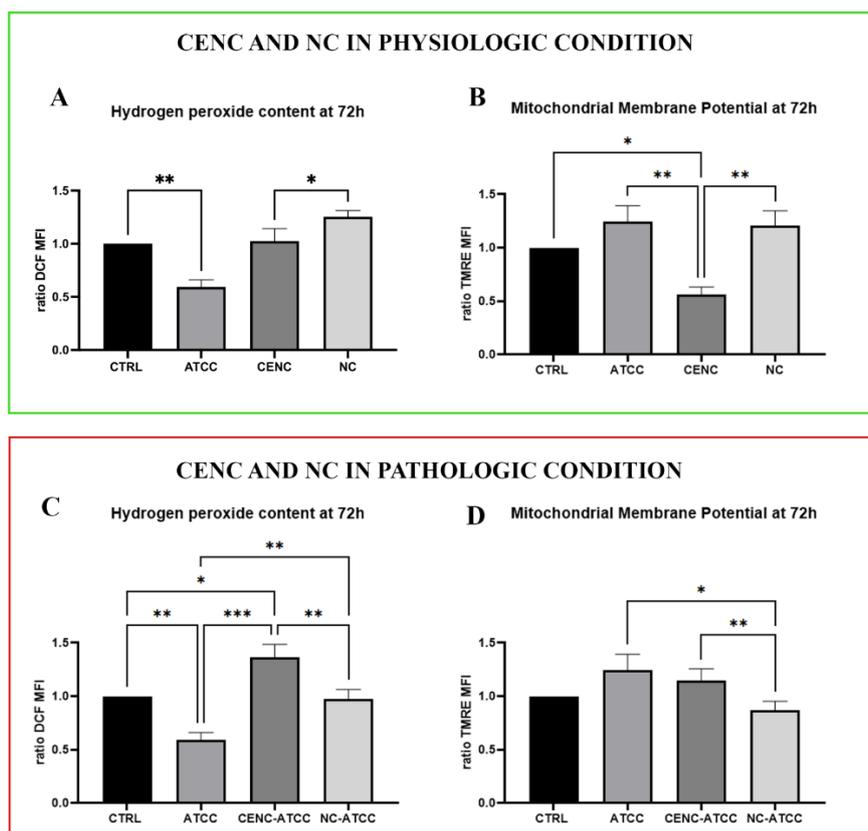
Figure 10. In the green square, ROS levels and MMP in physiological conditions: **(A)** statistical histogram of ROS levels at 72 h on HT-29 untreated cells (CTRL), ATCC treated cells, CENC and NC; expressed as fold of change of treated cells/CTRL cells of DCF MFI; **(B)** statistical histogram of MMP levels at 72 h on HT-29 untreated cells (CTRL), ATCC treated cells, CENC, and NC; expressed as fold of change of treated cells/CTRL cells of TMRE MFI. In the red square, ROS levels and MMP in pathological conditions: **(C)** statistical histogram of ROS levels at 72 h on HT-29 untreated cells (CTRL), ATCC treated cells, ATCC + CENC, and ATCC + NC; **(D)** statistical histogram of MMP levels at 72 h on HT-29 untreated cells (CTRL), ATCC treated cells, ATCC + CENC, and ATCC + NC. One-way ANOVA with Bonferroni's multiple comparison tests revealed significant differences (*$p < 0.05$, **$p < 0.01$, ***$p < 0.001$).

MMP highlighted a different response after CENC and NC administration in physiological conditions: a decrease and an increase, respectively (**Figure 10**). The pathologic condition panel highlights CENC and NC being able to lower the MMP rise induced by ATCC: the decrease is mild and not significant in CENC samples and more relevant and significant in NC samples.

Autophagic-like vesicles, actors of the autophagic process strictly linked to mitochondrial functions and ROS production [77], are traced by MDC labelling and quantified by flow cytometry. Our data did not point out any significant difference between the control, CENC, and NC samples; of note, the MFI increase observable in ATCC CDT-treated cells is reduced by both CENC and NC conditioning, reaching values like controls (**Figure 11A,D**).
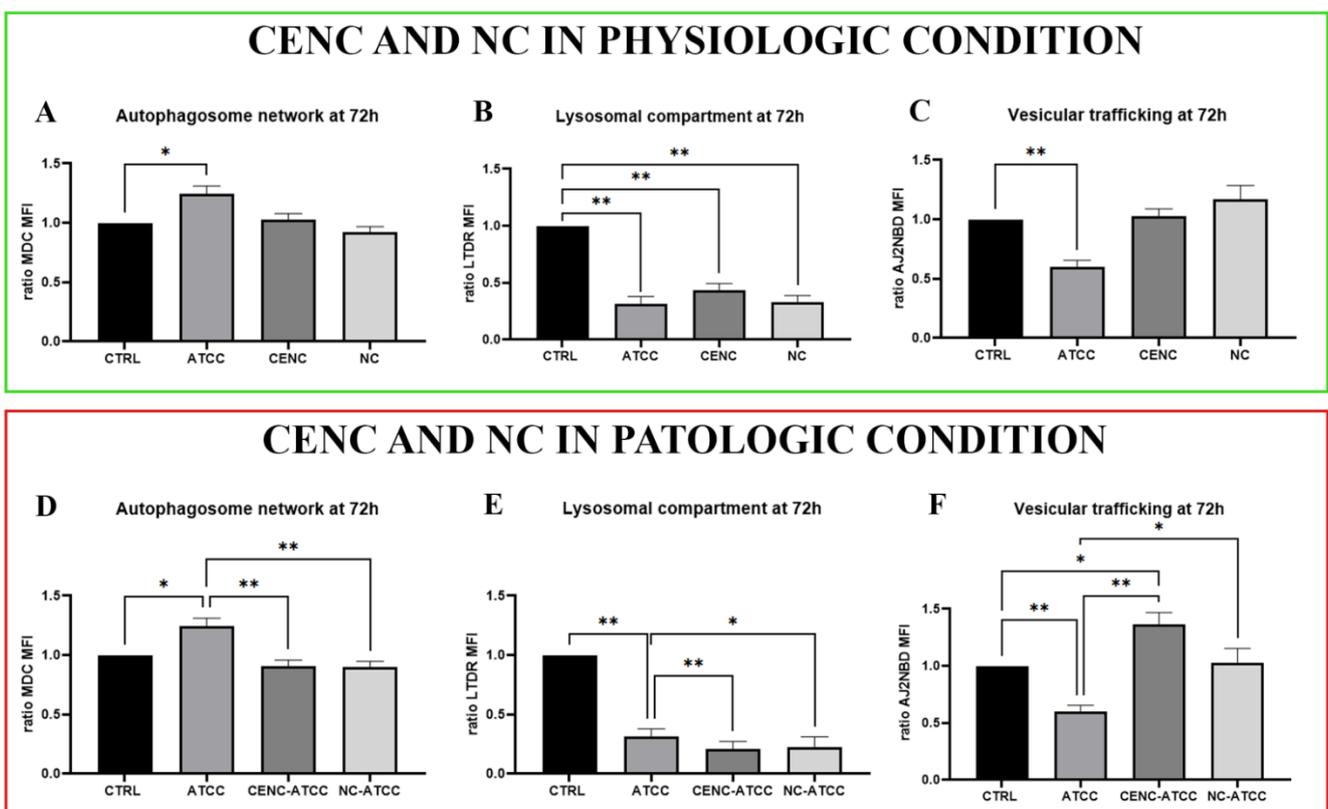
Figure 11. In the green square, the status of lysosomal and vesicular compartment in physiological conditions: **(A)** statistical histogram of autophagic-like vacuole at 72 h on HT-29 untreated cells (CTRL), ATCC treated cells CENC and NC; expressed as fold of change of treated cells/CTRL cells of MDC MFI; **(B)** statistical histogram of the lysosomal compartment at 72 h on HT-29 untreated cells (CTRL), ATCC treated cells, CENC and NC; expressed as fold of change of treated cells/CTRL cells of LTDR MFI; **(C)** statistical histogram of vesicular compartments at 72 h on HT-29 untreated cells (CTRL), ATCC treated cells, CENC and NC; expressed as fold of change of treated cells/CTRL cells of AJ2NBD MFI; In the red square, the status of lysosomal and vesicular compartment in pathological conditions; **(D)** statistical histogram of autophagic-like vacuole at 72 h on HT-29 untreated cells (CTRL), ATCC treated cells, CENC and NC; **(E)** statistical histogram of the lysosomal compartment at 72 h on HT-29 untreated cells (CTRL), ATCC treated cells, CENC and NC; **(F)** statistical histogram of vesicular compartments at 72 h on HT-29 untreated cells (CTRL), ATCC treated cells, ATCC + CENC, and ATCC + NC. One-way ANOVA with Bonferroni's multiple comparison tests revealed significant differences (*$p < 0.05$, **$p < 0.01$, ***$p < 0.001$).

We found significant differences for NC and CENC treatments in physiological conditions for lysosomes (LTDR MFI): both nanocellulose conditioning induced a relevant decrease compared to control and ATCC CDT-treated samples (**Figure 11B,E**). Given the high interconnectivity of endosomal, lysosomal, and autophagosomal pathways, dysfunctions in one of these systems may trigger alterations in another [78]. Briefly, the more acidic vacuoles, such as lysosomes, progressively decreased, from 24 h to 72 h in each ATCC CDT-treated sample, whereas after CENC treatments we observed an initial lysosome number/function increase (at 24 h), followed by a subsequent decrease (at 72 h). This finding is in agreement with other researchers [79,80] at least for the bioactive compound caffeine. Regarding non-acidic vacuoles targeted by AJ2NBD, a drop was detected after the 72 h treatment with ATCC, whereas CENC and NC seem to contribute, at any time points, to restoring the vesicle compartment (and trafficking) altered by ATCC CDT (**Figure 11C,F**).

The following scenario emerges from the data: i) after 24 h, NC and CENC treatments did not produce any relevant and significant modification; ii) ATCC-treated cells, as expected, revealed perturbations in the autophagic flux (increased autophagolysosomes and decreased acidic, mature lysosomes); iii) CENC and NC preconditioning restored autophagic vacuoles to the values of control cells, revealing a partial improvement of the perturbed autophagic flux.

4. Discussion and conclusion

Nanocellulose in food packaging applications, like any other food contact material, raises potential safety concerns [81]. Several review studies on NC have shown that toxicity studies remain scarce and knowledge gaps remain. Studies of nanocellulose exposure in various in vitro cell lines and animal models are limited, and no evidence of significant toxicity has been found [82], but certain studies have shown diverging results [83]. Our study is then useful to identify the properties of coffee-embedded nanocellulose and nanocellulose from coffee pods in an in vitro model represented by HT-29 intestinal cells.

The in vitro toxicological endpoints evaluated in this study consider cell death, ROS production (often an early precursor of cytotoxicity), mitochondria membrane potential, lysosomes, and autophagosomes. These approaches allowed to detect: i) mitochondrial damage, a crucial event in particulate matter (PM)-induced cytotoxicity [84]; ii) lysosomal network impairment; and iii) endosome and autophagosome alteration. In fact, endocytosis and autophagy are two major pathways for cellular homeostasis, and although endosomal and autophagy are discrete pathways, there is extensive crosstalk between these vesicular compartments.

The initial response to PM is a decrease in mitochondrial membrane potential and increased oxygen radical production, followed by inner mitochondrial membrane damage [85]. Our data reveal a mild decrease in MMP of CENC-treated cells after 72, but with CDT administration, MMP restores to the control level. These findings confirm that, also in our model and at the massive concentrations employed, both CENC and NC are non-cytotoxic. Furthermore, the three different interrelated intracellular vacuole/vesicle compartments analysed highlight the improvement of the

autophagic flux due to CENC and NC conditioning, suggesting the increase of non-acidic vacuoles (i.e., endosomes). In conclusion, the micro/nanoscaled cellulose in both CENC and NC formats from coffee pods does not significantly impact the viability and functions of HT-29 intestinal cells but does indeed improve the viable status and endosomal compartment after *C. jejuni* CDT intoxication.

However, results obtained from in vitro studies cannot often be used directly to predict the biological responses of organisms to chemical exposure in vivo. Therefore, further studies are needed, including chronic in vivo feeding studies and assessments of other potential endpoints.

Supplementary materials: Figures S1 and **S2** can be downloaded at Supplementary material.

Author contributions: Conceptualization, BC, MM and DL; methodology, DL, MM, BC, GP, MG, PG, LV, EM and DP; validation, DL, GP, MM and BC; formal analysis, DL, BC and MM; investigation, DL, BC, GP, EM and MM; resources, VF, SP and BC; data curation, DL, GP, MM, BC, LV and MG; writing—original draft preparation, DL, MM, BC and GP; writing—review and editing, DL, PG, MG, VL, EM, BC and MM; visualization, BC and DL; supervision, BC, DL and MM; project administration, BC and DL; funding acquisition, VF, SP and BC. All authors have read and agreed to the published version of the manuscript.

Conflict of interest: The authors declare no conflict of interest.

References

1. Athinarayanan J, Periasamy VS, Alsaif MA, et al. Presence of nanosilica (E551) in commercial food products: TNF-mediated oxidative stress and altered cell cycle progression in human lung fibroblast cells. Cell Biology and Toxicology. 2014; 30(2): 89-100. doi: 10.1007/s10565-014-9271-8
2. Gómez HC, Serpa A, Velásquez-Cock J, et al. Vegetable nanocellulose in food science: A review. Food Hydrocolloids. 2016; 57: 178-186. doi: 10.1016/j.foodhyd.2016.01.023
3. Khare S, DeLoid GM, Molina RM, et al. Effects of ingested nanocellulose on intestinal microbiota and homeostasis in Wistar Han rats. NanoImpact. 2020; 18: 100216. doi: 10.1016/j.impact.2020.100216
4. Onyango C, Unbehend G, Lindhauer MG. Effect of cellulose-derivatives and emulsifiers on creep-recovery and crumb properties of gluten-free bread prepared from sorghum and gelatinised cassava starch. Food Research International. 2009; 42(8): 949-955. doi: 10.1016/j.foodres.2009.04.011
5. Pereda M, Amica G, Rácz I, et al. Structure and properties of nanocomposite films based on sodium caseinate and nanocellulose fibers. Journal of Food Engineering. 2011; 103(1): 76-83. doi: 10.1016/j.jfoodeng.2010.10.001
6. Boluk Y, Lahiji R, Zhao L, et al. Suspension viscosities and shape parameter of cellulose nanocrystals (CNC). Colloids and Surfaces A: Physicochemical and Engineering Aspects. 2011; 377(1-3): 297-303. doi: 10.1016/j.colsurfa.2011.01.003
7. Kalashnikova I, Bizot H, Cathala B, et al. New Pickering Emulsions Stabilized by Bacterial Cellulose Nanocrystals. Langmuir. 2011; 27(12): 7471-7479. doi: 10.1021/la200971f
8. Zhao GH, Kapur N, Carlin B, et al. Characterisation of the interactive properties of microcrystalline cellulose-carboxymethyl cellulose hydrogels. International Journal of Pharmaceutics. 2011; 415(1-2): 95-101. doi: 10.1016/j.ijpharm.2011.05.054

9. Tang L, Huang B, Lu Q, et al. Ultrasonication-assisted manufacture of cellulose nanocrystals esterified with acetic acid. Bioresource Technology. 2013; 127: 100-105. doi: 10.1016/j.biortech.2012.09.133

10. Paunonen SV, Hong RY. The many faces of assumed similarity in perceptions of personality. Journal of Research in Personality. 2013; 47(6): 800-815. doi: 10.1016/j.jrp.2013.08.007

11. Alves JS, dos Reis KC, Menezes EGT, et al. Effect of cellulose nanocrystals and gelatin in corn starch plasticized films. Carbohydrate Polymers. 2015; 115: 215-222. doi: 10.1016/j.carbpol.2014.08.057

12. Nsor-Atindana J, Chen M, Goff HD, et al. Functionality and nutritional aspects of microcrystalline cellulose in food. Carbohydrate Polymers. 2017; 172: 159-174. doi: 10.1016/j.carbpol.2017.04.021

13. Robson AA. Tackling obesity: can food processing be a solution rather than a problem? Agro Food Industry Hi-Tech. 2012; 23(2): 10-11.

14. Cao X, Zhang T, DeLoid GM, et al. Cytotoxicity and cellular proteome impact of cellulose nanocrystals using simulated digestion and an in vitro small intestinal epithelium cellular model. NanoImpact. 2020; 20: 100269. doi: 10.1016/j.impact.2020.100269

15. Li Q, Wu Y, Fang R, et al. Application of Nanocellulose as particle stabilizer in food Pickering emulsion: Scope, Merits and challenges. Trends in Food Science & Technology. 2021; 110: 573-583. doi: 10.1016/j.tifs.2021.02.027

16. DeLoid GM, Cao X, Molina RM, et al. Toxicological effects of ingested nanocellulose in in vitro intestinal epithelium and in vivo rat models. Environmental Science: Nano. 2019; 6(7): 2105-2115. doi: 10.1039/c9en00184k

17. Karimian A, Parsian H, Majidinia M, et al. Nanocrystalline cellulose: Preparation, physicochemical properties, and applications in drug delivery systems. International Journal of Biological Macromolecules. 2019; 133: 850-859. doi: 10.1016/j.ijbiomac.2019.04.117

18. Lanfranchi M, Giannetto C, Dimitrova V. Evolutionary aspects of coffee consumers' buying habits: Results of a sample survey. Bulgarian Journal of Agricultural Science. 2016; 22(5): 705-712.

19. Abuabara L, Paucar-Caceres A, Burrowes-Cromwell T. Consumers' values and behaviour in the Brazilian coffee-in-capsules market: promoting circular economy. International Journal of Production Research. 2019; 57(23): 7269-7288. doi: 10.1080/00207543.2019.1629664

20. Chen H, Xu L, Yu K, et al. Release of microplastics from disposable cups in daily use. Science of The Total Environment. 2023; 854: 158606. doi: 10.1016/j.scitotenv.2022.158606

21. Corlett D, Stock Phot A. Nanoplastic should be better understood. Nature Nanotechnology. 2019; 14(4): 299-299. doi: 10.1038/s41565-019-0437-7

22. Cox KD, Covernton GA, Davies HL, et al. Human Consumption of Microplastics. Environmental Science & Technology. 2019; 53(12): 7068-7074. doi: 10.1021/acs.est.9b01517

23. Zangmeister CD, Radney JG, Benkstein KD, et al. Common Single-Use Consumer Plastic Products Release Trillions of Sub-100 nm Nanoparticles per Liter into Water during Normal Use. Environmental Science & Technology. 2022; 56(9): 5448-5455. doi: 10.1021/acs.est.1c06768

24. Rodríguez-Fabià S, Torstensen J, Johansson L, et al. Hydrophobisation of lignocellulosic materials part I: physical modification. Cellulose. 2022; 29(10): 5375-5393. doi: 10.1007/s10570-022-04620-8

25. Torstensen J, Ottesen V, Rodríguez-Fabià S, et al. The influence of temperature on cellulose swelling at constant water density. Scientific Reports. 2022; 12(1). doi: 10.1038/s41598-022-22092-5

26. Dagnon KL, Shanmuganathan K, Weder C, et al. Water-Triggered Modulus Changes of Cellulose Nanofiber Nanocomposites with Hydrophobic Polymer Matrices. Macromolecules. 2012; 45(11): 4707-4715. doi: 10.1021/ma300463y

27. Liu L, Kong F. The behavior of nanocellulose in gastrointestinal tract and its influence on food digestion. Journal of Food Engineering. 2021; 292: 110346. doi: 10.1016/j.jfoodeng.2020.110346

28. Salatin S, Yari Khosroushahi A. Overviews on the cellular uptake mechanism of polysaccharide colloidal nanoparticles. Journal of Cellular and Molecular Medicine. 2017; 21(9): 1668-1686. doi: 10.1111/jcmm.13110

29. Wang T, Bai J, Jiang X, et al. Cellular Uptake of Nanoparticles by Membrane Penetration: A Study Combining Confocal Microscopy with FTIR Spectroelectrochemistry. ACS Nano. 2012; 6(2): 1251-1259. doi: 10.1021/nn203892h

30. Crater JS, Carrier RL. Barrier Properties of Gastrointestinal Mucus to Nanoparticle Transport. Macromolecular Bioscience. 2010; 10(12): 1473-1483. doi: 10.1002/mabi.201000137

31. Bergin IL, Witzmann FA. Nanoparticle toxicity by the gastrointestinal route: evidence and knowledge gaps. International Journal of Biomedical Nanoscience and Nanotechnology. 2013; 3(1/2): 163. doi: 10.1504/ijbnn.2013.054515

32. Suvarna V, Nair A, Mallya R, et al. Antimicrobial Nanomaterials for Food Packaging. Antibiotics. 2022; 11(6): 729. doi: 10.3390/antibiotics11060729

33. Bintsis T. Foodborne pathogens. AIMS Microbiology. 2017; 3(3): 529-563. doi: 10.3934/microbiol.2017.3.529

34. Canonico B, Cesarini E, Montanari M, et al. Rapamycin Re-Directs Lysosome Network, Stimulates ER-Remodeling, Involving Membrane CD317 and Affecting Exocytosis, in Campylobacter Jejuni-Lysate-Infected U937 Cells. International Journal of Molecular Sciences. 2020; 21(6): 2207. doi: 10.3390/ijms21062207

35. Pickett CL, Pesci EC, Cottle DL, et al. Prevalence of cytolethal distending toxin production in Campylobacter jejuni and relatedness of Campylobacter sp. cdtB gene. Infection and Immunity. 1996; 64(6): 2070-2078. doi: 10.1128/iai.64.6.2070-2078.1996

36. Lara-Tejero M, Galán JE. A Bacterial Toxin That Controls Cell Cycle Progression as a Deoxyribonuclease I-Like Protein. Science. 2000; 290(5490): 354-357. doi: 10.1126/science.290.5490.354

37. Zhang Y, Huang R, Jiang Y, et al. The role of bacteria and its derived biomaterials in cancer radiotherapy. Acta Pharmaceutica Sinica B. 2023; 13(10): 4149-4171. doi: 10.1016/j.apsb.2022.10.013

38. Canonico B, Campana R, Luchetti F, et al. Campylobacter jejuni cell lysates differently target mitochondria and lysosomes on HeLa cells. Apoptosis. 2014; 19(8): 1225-1242. doi: 10.1007/s10495-014-1005-0

39. Canonico B, Di Sario G, Cesarini E, et al. Monocyte Response to Different Campylobacter jejuni Lysates Involves Endoplasmic Reticulum Stress and the Lysosomal-Mitochondrial Axis: When Cell Death Is Better Than Cell Survival. Toxins. 2018; 10(6): 239. doi: 10.3390/toxins10060239

40. Jongsma MLM, Berlin I, Wijdeven RHM, et al. An ER-Associated Pathway Defines Endosomal Architecture for Controlled Cargo Transport. Cell. 2016; 166(1): 152-166. doi: 10.1016/j.cell.2016.05.078

41. Nasoni MG, Carloni S, Canonico B, et al. Melatonin reshapes the mitochondrial network and promotes intercellular mitochondrial transfer via tunneling nanotubes after ischemic-like injury in hippocampal HT22 cells. Journal of Pineal Research. 2021; 71(1). doi: 10.1111/jpi.12747

42. Canonico B, Cangiotti M, Montanari M, et al. Characterization of a fluorescent 1,8-naphthalimide-functionalized PAMAM dendrimer and its Cu(ii) complexes as cytotoxic drugs: EPR and biological studies in myeloid tumor cells. Biological Chemistry. 2022; 403(3): 345-360. doi: 10.1515/hsz-2021-0388

43. Salucci S, Burattini S, Battistelli M, et al. Tyrosol prevents apoptosis in irradiated keratinocytes. Journal of Dermatological Science. 2015; 80(1): 61-68. doi: 10.1016/j.jdermsci.2015.07.002

44. Fiorani M, De Matteis R, Canonico B, et al. Temporal correlation of morphological and biochemical changes with the recruitment of different mechanisms of reactive oxygen species formation during human SW872 cell adipogenic differentiation. BioFactors. 2021; 47(5): 837-851. doi: 10.1002/biof.1769

45. Fusi V, Formica M, Giorgi L, et al. Preparation of heterocyclic compounds as fluorescent probes for detection in biological systems. Available online: https://ora.uniurb.it/handle/11576/2675836.2 (accessed on 5 January 2023).

46. Canonico B, Giorgi L, Nasoni MG, et al. Synthesis and biological characterization of a new fluorescent probe for vesicular trafficking based on polyazamacrocycle derivative. Biological Chemistry. 2021; 402(10): 1225-1237. doi: 10.1515/hsz-2021-0204

47. Tayeb A, Amini E, Ghasemi S, et al. Cellulose Nanomaterials—Binding Properties and Applications: A Review. Molecules. 2018; 23(10): 2684. doi: 10.3390/molecules23102684

48. Roman M, Winter WT. Effect of Sulfate Groups from Sulfuric Acid Hydrolysis on the Thermal Degradation Behavior of Bacterial Cellulose. Biomacromolecules. 2004; 5(5): 1671-1677. doi: 10.1021/bm034519

49. Čolić M, Tomić S, Bekić M. Immunological aspects of nanocellulose. Immunology Letters. 2020; 222: 80-89. doi: 10.1016/j.imlet.2020.04.004

50. Pereira MM, Raposo NRB, Brayner R, et al. Cytotoxicity and expression of genes involved in the cellular stress response and apoptosis in mammalian fibroblast exposed to cotton cellulose nanofibers. Nanotechnology. 2013; 24(7): 075103. doi: 10.1088/0957-4484/24/7/075103

51. Oh JH, Lee JT, Yang ES, et al. The coffee diterpene kahweol induces apoptosis in human leukemia U937 cells through down-regulation of Akt phosphorylation and activation of JNK. Apoptosis. 2009; 14(11): 1378-1386. doi: 10.1007/s10495-009-0407-x

52. Jabir NR, Islam MT, Tabrez S, et al. An insight towards anticancer potential of major coffee constituents. BioFactors. 2018; 44(4): 315-326. doi: 10.1002/biof.1437

53. Prasanthi JRP, Dasari B, Marwarha G, et al. Caffeine protects against oxidative stress and Alzheimer's disease-like pathology in rabbit hippocampus induced by cholesterol-enriched diet. Free Radical Biology and Medicine. 2010; 49(7): 1212-1220. doi: 10.1016/j.freeradbiomed.2010.07.007

54. Ko J, Kim JY, Kim J, et al. Anti-oxidative and anti-adipogenic effects of caffeine in an in vitro model of Graves' orbitopathy. Endocrine Journal. 2020; 67(4): 439-447. doi: 10.1507/endocrj.ej19-0521

55. Silvério A dos SD, Pereira RGFA, Duarte SM da S, et al. Coffee beverage reduces ROS production and does not affect the organism s response against Candida albicans. Revista de Ciências Farmacêutica Básica e Aplicadas—RCFBA. 2020; 41. doi: 10.4322/2179-443x.0684

56. Castaldo L, Toriello M, Sessa R, et al. Antioxidant and Anti-Inflammatory Activity of Coffee Brew Evaluated after Simulated Gastrointestinal Digestion. Nutrients. 2021; 13(12): 4368. doi: 10.3390/nu13124368

57. To EE, Erlich JR, Liong F, et al. Therapeutic Targeting of Endosome and Mitochondrial Reactive Oxygen Species Protects Mice from Influenza Virus Morbidity. Frontiers in Pharmacology. 2022; 13: 870156. doi: 10.3389/fphar.2022.870156

58. Zeng Q, Ma X, Song Y, et al. Targeting regulated cell death in tumor nanomedicines. Theranostics. 2022; 12(2): 817-841. doi: 10.7150/thno.67932

59. Amatori S, Ambrosi G, Borgogelli E, et al. Modulating the Sensor Response to Halide Using NBD-Based Azamacrocycles. Inorganic Chemistry. 2014; 53(9): 4560-4569. doi: 10.1021/ic5001649

60. Miękus N, Marszałek K, Podlacha M, et al. Health Benefits of Plant-Derived Sulfur Compounds, Glucosinolates, and Organosulfur Compounds. Molecules. 2020; 25(17): 3804. doi: 10.3390/molecules25173804

61. Xie J, Liao B, Tang RY. Functional Application of Sulfur-Containing Spice Compounds. Journal of Agricultural and Food Chemistry. 2020; 68(45): 12505-12526. doi: 10.1021/acs.jafc.0c05002

62. Cano-Marquina A, Tarín JJ, Cano A. The impact of coffee on health. Maturitas. 2013; 75(1): 7-21. doi: 10.1016/j.maturitas.2013.02.002

63. Montanari M, Guescini M, Gundogdu O, et al. Extracellular Vesicles from Campylobacter jejuni CDT-Treated Caco-2 Cells Inhibit Proliferation of Tumour Intestinal Caco-2 Cells and Myeloid U937 Cells: Detailing the Global Cell Response for Potential Application in Anti-Tumour Strategies. International Journal of Molecular Sciences. 2022; 24(1): 487. doi: 10.3390/ijms24010487

64. Hickey TE, Majam G, Guerry P. Intracellular Survival of Campylobacter jejuni in Human Monocytic Cells and Induction of Apoptotic Death by Cytolethal Distending Toxin. Infection and Immunity. 2005; 73(8): 5194-5197. doi: 10.1128/iai.73.8.5194-5197.2005

65. Alzheimer M, Svensson SL, König F, et al. A three-dimensional intestinal tissue model reveals factors and small regulatory RNAs important for colonization with Campylobacter jejuni. PLOS Pathogens. 2020; 16(2): e1008304. doi: 10.1371/journal.ppat.1008304

66. Martin OCB, Frisan T. Bacterial Genotoxin-Induced DNA Damage and Modulation of the Host Immune Microenvironment. Toxins. 2020; 12(2): 63. doi: 10.3390/toxins12020063

67. Balta I, Butucel E, Stef L, et al. Anti-Campylobacter Probiotics: Latest Mechanistic Insights. Foodborne Pathogens and Disease. 2022; 19(10): 693-703. doi: 10.1089/fpd.2022.0039

68. Athinarayanan J, Alshatwi AA, Subbarayan Periasamy V. Biocompatibility analysis of Borassus flabellifer biomass-derived nanofibrillated cellulose. Carbohydrate Polymers. 2020; 235: 115961. doi: 10.1016/j.carbpol.2020.115961

69. Ventura C, Pinto F, Lourenço AF, et al. On the toxicity of cellulose nanocrystals and nanofibrils in animal and cellular models. Cellulose. 2020; 27(10): 5509-5544. doi: 10.1007/s10570-020-03176-9

70. Wang X, Qiu Y, Wang M, et al. Endocytosis and Organelle Targeting of Nanomedicines in Cancer Therapy. International Journal of Nanomedicine. 2020; 15: 9447-9467. doi: 10.2147/ijn.s274289

71. López-Galilea I, De Peña MP, Cid C. Correlation of Selected Constituents with the Total Antioxidant Capacity of Coffee Beverages: Influence of the Brewing Procedure. Journal of Agricultural and Food Chemistry. 2007; 55(15): 6110-6117. doi: 10.1021/jf070779x

72. Acidri R, Sawai Y, Sugimoto Y, et al. Phytochemical Profile and Antioxidant Capacity of Coffee Plant Organs Compared to Green and Roasted Coffee Beans. Antioxidants. 2020; 9(2): 93. doi: 10.3390/antiox9020093

73. Andueza S, Cid C, Cristina Nicoli M. Comparison of antioxidant and pro-oxidant activity in coffee beverages prepared with conventional and "Torrefacto" coffee. LWT—Food Science and Technology. 2004; 37(8): 893-897. doi: 10.1016/j.lwt.2004.04.004

74. Cui WQ, Wang ST, Pan D, et al. Caffeine and its main targets of colorectal cancer. World Journal of Gastrointestinal Oncology. 2020; 12(2): 149-172. doi: 10.4251/wjgo.v12.i2.149

75. Lee C. Antioxidant ability of caffeine and its metabolites based on the study of oxygen radical absorbing capacity and inhibition of LDL peroxidation. Clinica Chimica Acta. 2000; 295(1-2): 141-154. doi: 10.1016/S0009-8981(00)00201-1

76. Soares MJ, Sampaio GR, Guizellini GM, et al. Regular and decaffeinated espresso coffee capsules: Unravelling the bioaccessibility of phenolic compounds and their antioxidant properties in milk model system upon in vitro digestion. LWT. 2021; 135: 110255. doi: 10.1016/j.lwt.2020.110255

77. Filomeni G, De Zio D, Cecconi F. Oxidative stress and autophagy: the clash between damage and metabolic needs. Cell Death & Differentiation. 2014; 22(3): 377-388. doi: 10.1038/cdd.2014.150

78. Roosen DA, Cookson MR. LRRK2 at the interface of autophagosomes, endosomes and lysosomes. Molecular Neurodegeneration. 2016; 11(1). doi: 10.1186/s13024-016-0140-1

79. Farias-Pereira R, Park CS, Park Y. Mechanisms of action of coffee bioactive components on lipid metabolism. Food Science and Biotechnology. 2019; 28(5): 1287-1296. doi: 10.1007/s10068-019-00662-0

80. Al-Bari MdAA, Ito Y, Ahmed S, et al. Targeting Autophagy with Natural Products as a Potential Therapeutic Approach for Cancer. International Journal of Molecular Sciences. 2021; 22(18): 9807. doi: 10.3390/ijms22189807

81. Silva FAGS, Dourado F, Gama M, et al. Nanocellulose Bio-Based Composites for Food Packaging. Nanomaterials. 2020; 10(10): 2041. doi: 10.3390/nano10102041

82. Bhattacharya K, Kiliç G, Costa PM, Fadeel B. Cytotoxicity screening and cytokine profiling of nineteen nanomaterials enables hazard ranking and grouping based on inflammogenic potential. Nanotoxicology. 2017; 11(6): 809-826. doi: 10.1080/17435390.2017.1363309

83. Stoudmann N, Schmutz M, Hirsch C, et al. Human hazard potential of nanocellulose: quantitative insights from the literature. Nanotoxicology. 2020; 14(9): 1241-1257. doi: 10.1080/17435390.2020.1814440

84. Hiura TS, Li N, Kaplan R, et al. The Role of a Mitochondrial Pathway in the Induction of Apoptosis by Chemicals Extracted from Diesel Exhaust Particles. The Journal of Immunology. 2000; 165(5): 2703-2711. doi: 10.4049/jimmunol.165.5.2703

85. Teodoro JS, Simões AM, Duarte FV, et al. Assessment of the toxicity of silver nanoparticles in vitro: A mitochondrial perspective. Toxicology in Vitro. 2011; 25(3): 664-670. doi: 10.1016/j.tiv.2011.01.004